

# Blind Image Deblurring using FFT-ReLU with Deep Learning Pipeline Integration

Abdul Mohaimen Al Radi<sup>1†</sup>, Prothito Shovon Majumder<sup>1\*†</sup>,  
Syed Mumtahir Mahmud<sup>1</sup>, Mahdi Mohd Hossain Noki<sup>1</sup>,  
Md. Haider Ali<sup>1</sup>, Md. Mosaddek Khan<sup>1</sup>

<sup>1\*</sup>Department of Computer Science and Engineering, University of Dhaka, Dhaka, 1000, Bangladesh.

\*Corresponding author(s). E-mail(s): [turnoshovon1999@gmail.com](mailto:turnoshovon1999@gmail.com);  
Contributing authors: [alradi9923@gmail.com](mailto:alradi9923@gmail.com); [syedmumtahir-2019617833@cs.du.ac.bd](mailto:syedmumtahir-2019617833@cs.du.ac.bd); [mahdimohdhossain-2019017785@cs.du.ac.bd](mailto:mahdimohdhossain-2019017785@cs.du.ac.bd);  
[haider@du.ac.bd](mailto:haider@du.ac.bd); [mosaddek@du.ac.bd](mailto:mosaddek@du.ac.bd);

<sup>†</sup>These authors contributed equally to this work.

## Abstract

Blind image deblurring is the process of deriving a sharp image and a blur kernel from a blurred image. Blurry images are typically modeled as the convolution of a sharp image with a blur kernel, necessitating the estimation of the unknown blur kernel to perform blind image deblurring effectively. Existing approaches primarily focus on domain-specific features of images, such as salient edges, dark channels, and light streaks. These features serve as probabilistic priors to enhance the estimation of the blur kernel. For improved generality, we propose a novel prior (ReLU sparsity prior) that estimates blur kernel effectively across all distributions of images (natural, facial, text, low-light, saturated etc). Our approach demonstrates superior efficiency, with inference times up to three times faster, while maintaining high accuracy in PSNR, SSIM, and error ratio metrics. We also observe noticeable improvement in the performance of the state-of-the-art architectures (in terms of aforementioned metrics) in deep learning based approaches when our method is used as a post-processing unit.

**Keywords:** Image restoration, Fast Fourier Transform, Kernel estimation, Blind deconvolution



Fig. 1: Results of our blind image deblurring algorithm on two blurry images

## 1 Introduction

Blind image deblurring is a classical problem in the fields of image and signal processing, and has been a subject of active research in the fields of computer vision. With more and more handheld devices being used to capture photos every day, blurring has become a significant source of degradation of image quality. The types of blur encountered include Gaussian blur, motion blur, out-of-focus blur, atmospheric blur, and others. Motion blur and out-of-focus blur are identified as the primary sources of blur in image restoration.

The objective of blind image deblurring is to estimate a blur kernel and a latent sharp image from the input blurry image. In the case of spatially invariant and uniform blur, the process of blurring can be expressed as follows:

$$B = I \otimes K + n$$

where  $B$  is the input blurry image,  $I$  is the latent sharp image,  $\otimes$  denotes convolution,  $K$  is the blur kernel i.e. the point spread function (PSF) controlling the degree of distortion of the image, and  $n$  is the additional noise that is gathered during image acquisition. Since the only available input is  $B$ , the problem becomes ill-posed: many pairs of  $I$  and  $K$  can produce the same  $B$ .

A common approach taken in blind image deblurring is the maximum a posteriori (MAP) framework, where the latent image and the blur kernel are optimized simultaneously in turns. Different assumptions or heuristics involving the latent image, the kernel, or both are used in such frameworks from [Chan and Wong \(1998\)](#); [Fergus, Singh, Hertzmann, Roweis, and Freeman \(2006\)](#); [Krishnan, Tay, and Fergus \(2011\)](#); [Levin, Weiss, Durand, and Freeman \(2011\)](#); [J. Pan, Hu, Su, and Yang \(2014b\)](#); [Shan, Jia, and Agarwala \(2008\)](#); [Xu, Zheng, and Jia \(2013\)](#), designing new priors that provide effective results. However, these methods are generally handcrafted for images from individual domains, such as the work of [J. Pan et al. \(2014b\)](#), since they build on image-specific properties that aid in optimization techniques. Moreover, the calculation of some of these priors can incur high computational costs, as noted by ([J. Pan, Sun, Pfister, & Yang, 2016](#)), which may reduce the effectiveness in deblurring images.

Since the blur kernel and the latent image are typically solved in an alternating fashion, the initialization steps play a vital role in the convergence of any deblurring algorithm. In the frequency domain, the blurred image is instantiated as the multiplications of the Fourier transforms of the latent image and the blur kernel (PSF), added with sensor noise, as proposed in [Chakrabarti, Zickler, and Freeman \(2010\)](#); [Hu, Cho, Wang, and Yang \(2014\)](#); [J. Pan et al. \(2016\)](#); [Xu et al. \(2013\)](#).

$$B(\omega) = I(\omega)K(\omega) + N(\omega)$$

where  $B(\omega)$ ,  $I(\omega)$ ,  $K(\omega)$  and  $N(\omega)$  represent Fourier transforms of the blurry image, the latent sharp image, the blur kernel, and the sensor noise, respectively, and  $\omega \in [-\pi, \pi]^2$ . [Z. Li, Gao, Yi, Fu, and Chen \(2023\)](#) depicts that a series of Fourier Transform, ReLU, and Inverse Fourier Transform operations can implicitly reveal faithful information about the blur kernel, such as the direction and the level of the blur. They proposed a Res FFT-ReLU block for performing these operations, which can be placed and used in existing architectures based on neural networks. However, its applications in blind image deblurring remained unexplored.

In this paper, we propose a new prior, the ReLU Sparsity prior. A sharp image has a higher number of zero elements compared to its blurry counterpart, which is a property that can lead to producing the latent image, as shown empirically in our work. Besides, we refer to the aforementioned sequence of operations together as RFT and use its  $L_0$  norm in our prior. Minimizing the objective function would necessarily imply penalizing the lower sparsity of the blurry image. Since an  $L_0$  norm is involved, we use the half quadratic splitting technique, [Xu, Lu, Xu, and Jia \(2011\)](#), to optimize our objective function.

Another unexplored field of research within the domain of Image Deblurring, in general, is the combination of traditional blind deconvolution methods with deep learning architectures. This gap exists because no previous work has implemented a blind deconvolution method that can be seamlessly applied to transformer-based deep learning architectures. We have mitigated this issue by implementing our method in a pipeline that is suitable for incorporating deep learning.

Our main contributions are summarized as follows:

1. We propose a new prior, the ReLU Sparsity prior, which allows us to obtain faithful information about the blur kernel regardless of the nature of the image, while simultaneously applying optimization techniques based on the change in sparsity that occurs due to convolution. [Fig. 1](#) is an example of deblurred output from our algorithm.
2. Our algorithm achieves competitive performance based on the PSNR, SSIM and error ratio metrics when compared with state-of-the-art blind image deblurring algorithms from [S. Cho and Lee \(2009\)](#); [Fergus et al. \(2006\)](#); [Krishnan et al. \(2011\)](#); [J. Pan et al. \(2016\)](#); [L. Pan, Hartley, Liu, and Dai \(2019\)](#); [Shan et al. \(2008\)](#); [Xu and Jia \(2010\)](#), while achieving significantly lower inference time on high-resolution images when compared using images from benchmark datasets prepared by [Köhler, Hirsch, Mohler, Scholkopf, and Harmeling \(2012\)](#); [Levin, Weiss, Durand, and Freeman \(2009\)](#).

3. We employed our algorithm as a post-processing unit for currently established state-of-the-art methods listed in the literature, including [L. Chen, Chu, Zhang, and Sun \(2022\)](#); [Kupyn, Budzan, Mykhailych, Mishkin, and Matas \(2018\)](#); [Kupyn, Martyniuk, Wu, and Wang \(2019\)](#); [Tsai, Peng, Lin, Tsai, and Lin \(2022\)](#); [Zamir, Arora, Hayat, Khan, and Yang \(2022\)](#); [Zamir et al. \(2021\)](#); [H. Zhang, Dai, Li, and Koniusz \(2019\)](#), specifically for the RealBlur dataset from [Rim, Haeyun, Won, and Cho \(2020\)](#). We observed notable improvements in the aforementioned metrics when compared with these works standalone, i.e., without any post-processing units.

## 2 Related Works

Due to the joint estimation of the blur kernel and the latent sharp image from the input blurry image, single-image deblurring is an under-constrained problem, which is typically formulated in MAP frameworks, such as [Mao, Liu, and Li \(2018\)](#). Initial advances relied on statistical priors and salient edge detection, such as [S. Cho and Lee \(2009\)](#); [Fergus et al. \(2006\)](#); [Krishnan et al. \(2011\)](#); [Levin et al. \(2011\)](#); [Shan et al. \(2008\)](#); [Xu and Jia \(2010\)](#); [Xu et al. \(2013\)](#), although the existence of strong edges in latent images is not guaranteed.

Different image priors and likelihood estimations have been proposed to improve the efficiency of MAP frameworks. Such regularizations or assumptions about the blur kernel or the latent image include  $L_0$  regularized prior by [J. Pan et al. \(2014b\)](#); [Xu, Tao, and Jia \(2014\)](#), by dark channel prior [J. Pan et al. \(2016\)](#), extreme channel prior by [Yan, Ren, Guo, Wang, and Cao \(2017\)](#), patch prior by [Ljubenović and Figueiredo \(2017\)](#), local binary pattern prior by [Z. Zhang et al. \(2022\)](#), latent structure prior by [Bai et al. \(2019\)](#), learned image prior by [L. Li et al. \(2018\)](#), uniform blur by [Levin et al. \(2009\)](#); [Xu et al. \(2013\)](#), local maximum difference prior by [Liu, Tan, He, Ge, and Hu \(2020\)](#), internal patch recurrence by [Michaeli and Irani \(2014\)](#), Laplacian prior by [X. Chen et al. \(2020\)](#), tri-segment intensity prior by [H. Zhang, Wu, Zhang, Zhang, and Li \(2020\)](#), graph-based image prior by [Bai, Cheung, Liu, and Gao \(2018\)](#), constant depth by [Gupta, Joshi, Zitnick, Cohen, and Curless \(2010\)](#); [Xu and Jia \(2012\)](#), in-plane rotation by [J. Sun, Cao, Xu, and Ponce \(2015\)](#), and forward motion by [Zheng, Xu, and Jia \(2013\)](#). [Fergus et al. \(2006\)](#) use variational Bayesian inference to learn an image gradient prior. [Levin et al. \(2009\)](#) show that this method can avoid trivial solutions that naive MAP-based methods can possibly be unable to.

Sparsity priors have been shown to be useful in kernel estimation in MAP frameworks. [Krishnan et al. \(2011\)](#) used normalized sparsity prior in their MAP framework for kernel estimation, [Xu and Jia \(2010\)](#) proposed a two-phase technique for deblurring single images: the estimation of blur kernel using edge selections and ISD optimizations is followed by non-blind deconvolution with total variation, with an additional Gaussian prior from [S. Cho and Lee \(2009\)](#).

Several newer approaches designed for domain-specific deblurring, such as low-illumination ([Hu et al., 2014](#)), text ([X. Chen, He, Yang, & Wu, 2011](#); [H. Cho, Wang, & Lee, 2012](#); [J. Pan et al., 2014b](#)) and face ([J. Pan, Hu, Su, & Yang, 2014a](#)) images utilize inherent statistical characteristics of their domains, but display a lack of generality when applied to natural images of other distributions.

Recent advancements in the research of deep learning resulted in the rise of designing neural networks tailored for the task of image restoration, including image deblurring. Besides datasets for blind deblurring algorithms such as Köhler et al. (2012), datasets were acquired for training and testing these neural networks as well, for example by Nah, Kim, and Lee (2017); Rim et al. (2020); Shen et al. (2019). Architectures based on CNNs utilised encoder-decoder structures from Kim, Lee, and Cho (2022); Tao, Gao, Shen, Wang, and Jia (2018); Zamir et al. (2021), while GANs made use of their generator-discriminator networks to produce clear images from blurred ones, as proposed by Kupyn et al. (2018, 2019); K. Zhang et al. (2020). Later on, architectures based on Transformers such as Wang et al. (2022) and Multilayer Perceptrons including Lee-Thorp, Ainslie, Eckstein, and Ontanon (2022); Rao, Zhao, Zhu, Lu, and Zhou (2021) also produced excellent results in image restoration.

The advent of deep learning has seen a decrease in new approaches utilising traditional techniques, and as a result, the inherent properties of images and the blurring process is overlooked. The earlier methods, often domain-specific, lack in generalisation; the objective of our research is to design a deblurring framework that combines the strength of these two streams and covers each other’s weakness.

### 3 ReLU Sparsity Prior

In this section, we discuss the sparsity property of applying RFT operation and develop the ReLU prior to formulate an objective function to estimate the latent sharp image and blur kernel. In Section 3.1, we explain the concept of sparsity and the RFT operations, and the connections between them. We define our model in Section 3.2. In the subsequent sections, we delve into the blind deconvolution and non-blind deconvolution aspects of our algorithm in further detail.

#### 3.1 Sparsity and RFT

To describe our work, we begin by discussing the effect of convolution on the sparsity of images. In standard deblurring models, blurry images are described as the result of convolving a sharp image with a blur kernel (Equation (1)). Here,  $(x, y)$  denotes the pixel location, and the blur kernel  $K$  has a size of  $k \times k$ .  $S$  and  $B$  are the sharp image and the blurry image, respectively.

$$B(x, y) = \sum_{i=0}^{k-1} \sum_{j=0}^{k-1} S(x+i, y+j) \cdot K(i, j) \quad (1)$$

Since the output of convolution represents a locally weighted linear combination of the input, it typically results in reduced sparsity. This means the output generally contains more nonzero elements due to the multiplicative and additive properties of convolution than the input. Therefore, a blurry image has fewer pixels which are very low in brightness. That is, it possesses more nonzero elements compared to the corresponding sharp image.

Now, We define the RFT as a function that processes an image through a series of steps: first, it computes the Fast Fourier Transform (FFT) of the image; then, it

applies the ReLU (Rectified Linear Unit) activation function to the FFT results; next, it calculates the inverse FFT of the activated data; finally, it subtracts half of the original image from this result to produce the final output.

$$RFT(I) = \mathcal{F}^{-1}(\text{ReLU}(\mathcal{F}(I))) - \frac{1}{2}I \quad (2)$$

Z. Li et al. (2023) show that by applying the aforementioned sequence of operations, faithful information about the blur pattern can be discovered, such as the direction and the level of blur. We observe that the sparsity properties of convolution are preserved even after applying the RFT operations. This observation enables us to penalize the nonzero results from RFT, as these indicate the presence of blur in the image. We apply the RFT operations from the dataset provided by L. Sun, Cho, Wang, and Hays (2013) and observe the values of  $L_0$  norm to empirically substantiate our observation in Fig. 2. We can observe the change in the  $L_0$  norm in blurry images compared to their sharp counterparts when the RFT operation is applied to both.

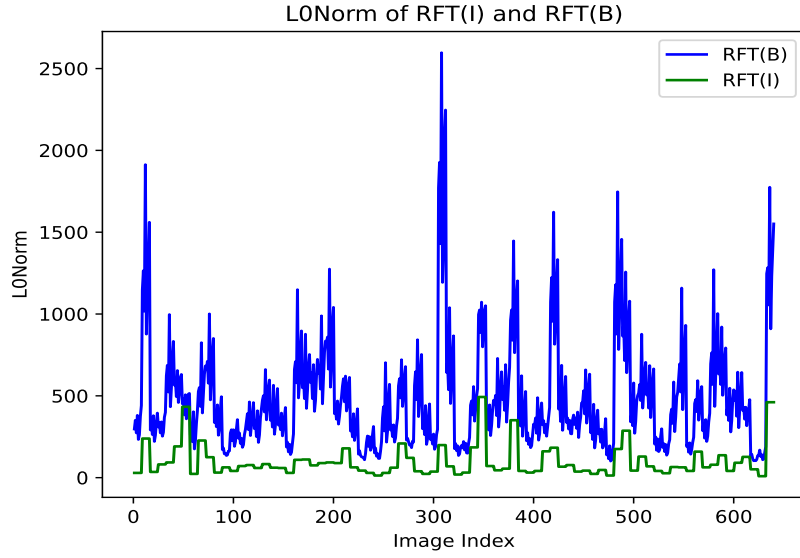


**Fig. 2:** Decreased Sparsity in Blurry Images after RFT

Here, we can clearly see that the  $L_0$  norm of RFT, when applied on blurry images, produces a higher value when compared to applying it on sharp ones.

### 3.2 Model and Optimization

Integrating  $RFT(I)$  to the standard formulation of image deblurring, we propose a novel objective function as follows:

$$\min_{I,k} \|I \otimes K - B\|_2^2 + \alpha \|k\|_2^2 + \beta \|\nabla I\|_0 + \lambda \|RFT(I)\|_0 \quad (3)$$

In this formulation, the first term ensures that the given blurred image and the convolution of the estimated latent image and blur kernels are as similar as possible. The second term applies regularization on the kernel. The third term retains large gradients and discards smaller ones, as discussed in [J. Pan et al. \(2014b\)](#); [Xu et al. \(2013\)](#). The parameters  $\alpha$ ,  $\beta$ , and  $\lambda$  serve as penalty coefficients. From Equation (3), we alternately solve for the latent image  $I$  and the blur kernel  $k$  using coordinate descent, employing the following equations respectively:

$$\min_I \|I \otimes k - B\|_2^2 + \beta \|\nabla I\|_0 + \lambda \|RFT(I)\|_0 \quad (4)$$

$$\min_k \|I \otimes k - B\|_2^2 + \alpha \|k\|_2^2 \quad (5)$$

### 3.3 Blind Deconvolution

In this section, we introduce the methodology for estimating the latent image  $I$  and the blur kernel  $k$  using the input blurry image  $B$ . This estimation process is fundamental to the recovery of the latent (sharp) image.

**Estimating  $I$ :** The non-linear  $RFT$  function and  $L_0$  regularisation make the minimization of Equation (4) challenging in terms of computation. Half-quadratic splitting methods from [Xu et al. \(2011\)](#) are used to handle  $L_0$  minimization. We split the gradients into  $g = (g_x, g_y)$  for gradients across x and y-axis, and introduce auxiliary variable  $h$  for  $RFT(I)$ . Rewriting Equation (4), we now have:

$$\min_{I,h,g} \|I \otimes k - B\|_2^2 + \gamma \|\nabla I - g\|_2^2 + \beta \|RFT(I) - h\|_2^2 + \mu \|g\|_0 + \lambda \|h\|_0 \quad (6)$$

where  $\gamma$  and  $\beta$  are penalty parameters. Solutions for individual variables ( $I$ ,  $u$ , or  $g$ ) can be calculated when the others are held constant. In order to use Equation (6) in Equation (1) to estimate the latent sharp image, we transform this in the frequency domain and reach a closed-form solution in Equations (10), (11), and (12).

In order to solve for the nonlinear  $RFT(I)$ , we observe that a linear operator  $\mathbf{F}$  can be used as a substitute when applied to the  $\mathbf{I}$  in vector form i.e. for the latent image,  $\mathbf{FI} = RFT(\mathbf{I})$ . To compute the values of  $\mathbf{F}$ , we use gradient descent with Adam optimizer. Using repeated reconstruction, we iteratively compute  $F$  from the previous estimation of  $I$ . We look at an example image pair from [Köhler et al. \(2012\)](#) and compare the rate of convergence across different number of steps in Fig. 3.

Given  $\mathbf{F}$ , we can solve for  $\mathbf{I}$  from:

$$\min_I \|\mathbf{T}_k \mathbf{I} - \mathbf{B}\|_2^2 + \gamma \|\nabla \mathbf{I} - \mathbf{g}\|_2^2 + \beta \|\mathbf{FI} - \mathbf{h}\|_2^2 \quad (7)$$



**Fig. 3:** Convergence of RFT

where  $\mathbf{T}_k$  is a Toeplitz matrix of  $k$ , which is multiplied with vectors using FFT  $\mathbf{B}$ ,  $\mathbf{g}$  and  $\mathbf{u}$  are denoted in their vector forms, respectively. The solution for Equation (7) is computed as follows:

$$\begin{aligned}
L &= \min_I \|\mathbf{T}_k \mathbf{I} - \mathbf{B}\|_2^2 + \gamma \|\nabla \mathbf{I} - \mathbf{g}\|_2^2 + \beta \|\mathbf{F} \mathbf{I} - \mathbf{h}\|_2^2 \\
&= (\mathbf{T}_k \mathbf{I} - \mathbf{B})^T (\mathbf{T}_k \mathbf{I} - \mathbf{B}) + \gamma (\nabla \mathbf{I} - \mathbf{g})^T (\nabla \mathbf{I} - \mathbf{g}) + \\
&\quad \beta (\mathbf{F} \mathbf{I} - \mathbf{h})^T (\mathbf{F} \mathbf{I} - \mathbf{h}) \\
&= \mathbf{I}^T \mathbf{T}_k^T \mathbf{T}_k \mathbf{I} - \mathbf{I}^T \mathbf{T}_k^T \mathbf{B} - \mathbf{B}^T \mathbf{T}_k^T \mathbf{I} + \mathbf{B}^T \mathbf{B} + \gamma \mathbf{I}^T \nabla^T \nabla \mathbf{I} - \gamma \mathbf{I}^T \nabla^T \mathbf{g} - \\
&\quad \gamma \mathbf{g}^T \nabla \mathbf{I} + \gamma \mathbf{g}^T \mathbf{g} + \beta \mathbf{I}^T \mathbf{F}^T \mathbf{F} \mathbf{I} - \beta \mathbf{I}^T \mathbf{F}^T \mathbf{h} - \beta \mathbf{h}^T \mathbf{F} \mathbf{I} + \beta \mathbf{h}^T \mathbf{h}
\end{aligned} \tag{8}$$

Here,  $\nabla = (\nabla_x, \nabla_y)$  represents the matrix for computing axiswise gradients. Differentiating Equation (8) with respect to  $I$ , we get:

$$\begin{aligned}
\frac{dL}{dI} &= 2\mathbf{T}_k^T \mathbf{T}_k \mathbf{I} - \mathbf{T}_k^T \mathbf{B} - \mathbf{T}_k^T \mathbf{B} + 0 + 2\gamma \nabla^T \nabla \mathbf{I} - \gamma \nabla^T \mathbf{g} - \gamma \nabla^T \mathbf{g} + 0 + \\
&\quad 2\beta \mathbf{F}^T \mathbf{F} \mathbf{I} - \beta \mathbf{F}^T \mathbf{h} - \beta \mathbf{F}^T \mathbf{h} \\
&= 2\mathbf{T}_k^T \mathbf{T}_k \mathbf{I} - 2\mathbf{T}_k^T \mathbf{B} + 2\gamma \nabla^T \nabla \mathbf{I} - 2\gamma \nabla^T \mathbf{g} + 2\beta \mathbf{F}^T \mathbf{F} \mathbf{I} - 2\beta \mathbf{F}^T \mathbf{h}
\end{aligned} \tag{9}$$

In the case of convergence,  $\frac{dL}{dI} = 0$ . Therefore,

$$\begin{aligned}
\mathbf{I} &= \frac{\mathbf{T}_k^T \mathbf{B} + \gamma \nabla^T \mathbf{g} + \beta \mathbf{F}^T \mathbf{h}}{\mathbf{T}_k^T \mathbf{T}_k + \gamma \nabla^T \nabla + \beta \mathbf{F}^T \mathbf{F}} \\
&= \mathcal{F}^{-1} \left( \frac{\overline{\mathcal{F}(\mathbf{K})} \mathcal{F}(\mathbf{B}) + \gamma \overline{\mathcal{F}(\nabla)} \mathcal{F}(\mathbf{g}) + \beta \overline{\mathcal{F}(\mathbf{F})} \mathcal{F}(\mathbf{h})}{\overline{\mathcal{F}(\mathbf{K})} \mathcal{F}(\mathbf{K}) + \gamma \overline{\mathcal{F}(\nabla)} \mathcal{F}(\nabla) + \beta \overline{\mathcal{F}(\mathbf{F})} \mathcal{F}(\mathbf{F})} \right)
\end{aligned} \tag{10}$$

Given  $\mathbf{I}$ , we can solve for  $h$  from:

$$\min_h \beta \|\mathbf{RFT}(\mathbf{I}) - h\|_2^2 + \lambda \|h\|_0 \tag{11}$$



and for  $g$  using element-wise minimization from:

$$\min_g \gamma \|\nabla I - g\|_2^2 + \mu \|g\|_0 \quad (12)$$

The solution for  $h$  can be written as:

$$h = \begin{cases} RFT(I), & |RFT(I)|^2 \geq \frac{\lambda}{\beta} \\ 0, & \text{otherwise} \end{cases} \quad (13)$$

The solution for  $g$  can also be written in a similar manner, using element-wise minimization techniques.

**Estimating  $k$ :** Solving Equation (5) becomes a least squares problem when  $I$  is fixed. Owing to the demonstrated effectiveness of gradient-based methods in kernel estimation, as detailed in [S. Cho and Lee \(2009\)](#); [Levin et al. \(2011\)](#); [Xu et al. \(2013\)](#), the kernel  $k$  is computed from:

$$\min_k \|\nabla I \otimes k - \nabla B\|_2^2 + \alpha \|k\|_2^2 \quad (14)$$

FFTs are used to solve Equation (14), using techniques mentioned in [S. Cho and Lee \(2009\)](#); [J. Pan et al. \(2014b\)](#); [Xu et al. \(2013\)](#). Negative elements of the kernel are set to zero, and the obtained kernel is then normalized.

---

**Algorithm 1:** Blind Deconvolution

---

**Input :**  $B$ : Blurry Image  
**Output:**  $I$ : Latent Image (Intermediate),  $k$ : Blur Kernel

- 1  $k \leftarrow$  initialised from coarse resolution
- 2  $scale \leftarrow$  computed according to  $k$
- 3 **for**  $i = 0$  **to**  $max\_scale$  **do**
- 4      $B_{intermediate} \leftarrow$   $downsample(B, scale)$
- 5     **for**  $j = 0$  **to**  $max\_iter$  **do**
- 6          $I \leftarrow$  solution of Equation (6)
- 7          $k \leftarrow$  solution of Equation (5)
- 8          $k \leftarrow$   $remove\_isolated\_noise(k)$
- 9          $k \leftarrow$   $adjust\_psf\_center(k)$
- 10     **end**
- 11      $k \leftarrow$   $estimate\_psf(k, scale)$
- 12      $scale \leftarrow scale + 1$
- 13 **end**
- 14 **return**  $I, k$

---

This blind deconvolution algorithm estimates the latent image  $I$  and the blur kernel  $k$ , which is necessary for obtaining the latent image. Initially, the kernel  $k$  is initialized to the coarsest resolution (line 1). Line 2 determines the scale according to

the current kernel size. The algorithm iteratively increases the scale. For each scale within a loop, the blurry image  $B$  is down-sampled to current scale in line 4. We iterate a predetermined number of times within this setting to refine estimation of  $I$  using Equation (6) in line 6, and  $k$  using Equation (5) in line 7. Isolated noises are removed by deleting connected components within the kernel that do not exceed a specified threshold (line 8). The kernel is centered after the noise removal in line 9. kernel is then up-sampled with the current scale in line 11. All down-sampling and up-sampling are done using bi-linear interpolation.

### 3.4 Non-blind Deconvolution

---

**Algorithm 2:** Non-blind Deconvolution

---

**Input** :  $I$ : Intermediate Latent Image,  $K$ : Intermediate Blur Kernel  
**Output**:  $I$ : Intermediate Latent Image with Ringing Artifacts Removed

```

1 for  $i = 0$  to  $num\_channels$  do
2   |  $I_c \leftarrow \text{laplacian\_prior\_estimation}(I_{channel_i})$ 
3   |  $I_1 \leftarrow \text{concatenate}(I_1, I_c)$ 
4 end
5  $I_2 \leftarrow$  solution for  $I$  using Equation (4)
6  $diff \leftarrow I_1 - I_2$ 
7  $I\_result \leftarrow I_1 - \text{bilateral\_filter}(diff)$ 
8 return  $I\_result$ 

```

---

For non-blind deconvolution, we estimate an image  $I_1$  with such priors in lines 2 and 3. Then, we use the  $L_0$  norm of the gradient from our Equation (4) to estimate another latent image  $I_2$  in line 5, since gradient-based methods have been shown to provide accurate results in suppressing ringing artifacts. Similar to ringing suppression methods discussed by Shan et al. (2008), we compute a difference map between these two estimated images in line 6. We use bilateral filtering on the computed difference map and subtract the result from  $I_1$  in line 7, thereby smoothing out artifacts and completing non-blind deconvolution.

## 4 Empirical Evaluation

This section discusses the parameter settings and provides quantitative results on datasets referenced from Köhler et al. (2012); Levin et al. (2009). Additionally, it presents visual results across various domains, including natural scenes, low-light conditions, text, and facial images. We also integrate our method as an add-on within a transformer-based deep learning framework and conduct comparative analyses.

## 4.1 Empirical Settings

We compare our results with both statistical deblurring algorithms (from S. Cho and Lee (2009); Fergus et al. (2006); Hirsch, Schuler, Harmeling, and Schölkopf (2011); Krishnan et al. (2011); J. Pan et al. (2016); Shan et al. (2008); Whyte, Sivic, Zisserman, and Ponce (2012); Xu et al. (2013)) and deep-learning based methods (from L. Chen et al. (2022); Kupyn et al. (2018, 2019); Tsai et al. (2022); Zamir et al. (2022, 2021); H. Zhang et al. (2019)), where our algorithm was used as a post-processing unit. The metrics chosen for the comparison include PSNR, SSIM, error ratio and inference time. In our experiments, the parameters  $\lambda$ ,  $\mu$  and  $\alpha$  are assigned values  $3 \times 10^{-4}$ , 0.004 and 2, respectively. We compared the convergence of the algorithm for various values of these parameters with respect to kernel similarity, and a more detailed analysis of this is provided in the supplementary material. The value of `max_iter` is set to be 5 as a trade-off between timing and precision. Our implementation for blind image deblurring on single images is done using Python.<sup>1</sup> Previous blind image deblurring work was mainly done in MATLAB, so translating it allows for GPU access and integration with deep learning techniques.

## 4.2 Benchmarking with Statistical Deblurring Algorithms

In this section, we evaluate our proposed algorithm with state-of-the-art statistical deblurring algorithms based on the metrics of PSNR, SSIM and error ratio, followed by a visual comparison with those algorithms.

### 4.2.1 Quantitative Results

We compare our results with others using images from Köhler et al. (2012) and Levin et al. (2009), employing PSNR, SSIM, error ratio and inference time as metrics.

**PSNR on Köhler et al. dataset:** We computed the average PSNR of our algorithm’s output across 32 images. For each of the 4 images and 8 kernels, there are 199 corresponding ground truth images used for PSNR calculation in Köhler et al. (2012), against other statistical deblurring algorithms.

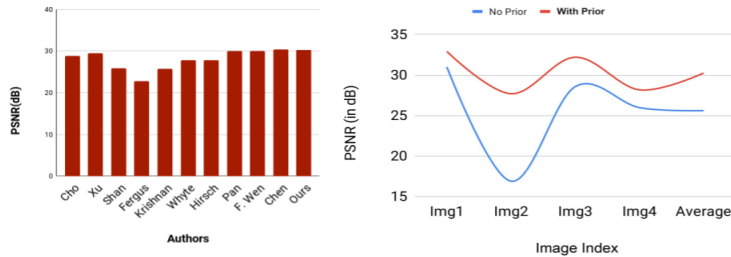


**Fig. 4:** Left: PSNR comparison with other algorithms, Right: PSNR with and without our prior

<sup>1</sup>The source code is available on the author’s GitHub pages.

We observe competitive performance when compared with the aforementioned algorithms, and the effect of the presence of our ReLU Sparsity Prior is also conspicuous in Fig. 4.

**Levin et al. dataset:** This dataset also contains 4 images and 8 kernels each. The images are grayscale and have dimensions of  $255 \times 255$ . We compare our PSNR, SSIM, error ratio, and inference times with the works in L. Chen, Fang, Wang, and Zhang (2019); S. Cho and Lee (2009); J. Pan et al. (2016); L. Pan et al. (2019); Wen, Ying, Liu, and Truong (2019).

	PSNR	SSIM	Error ratio	Average inference time
S. Cho and Lee (2009)	25.63	0.7907	2.6688	1.3951 seconds
J. Pan et al. (2016)	27.54	0.8626	1.2076	109.6088 seconds
L. Pan et al. (2019)	28.38	0.925	–	15.0949 seconds
Wen et al. (2019)	32.445	0.9344	–	18.61 seconds
L. Chen et al. (2019)	33.145	–	–	65.2 seconds
Ours	28.34	0.887	0.3475	8.057 seconds

**Table 1:** Comparison on Levin et al. dataset

In Table 1, we show that our method achieves the best error ratio, while achieving a reasonable tradeoff between inference time and PSNR/SSIM.

**Inference Time Comparison:** We compare our work with J. Pan et al. (2016) and L. Pan et al. (2019) in this section, using datasets from Köhler et al. (2012); Levin et al. (2009); L. Sun et al. (2013). The images in this datasets are of dimensions  $255 \times 255$ ,  $800 \times 800$  and  $1024 \times 800$ , respectively.

Algorithm	Inference Time (seconds)		
	Levin et al.	Köhler et al.	Sun et al.
J. Pan et al. (2016)	109.609	1550.932	2280.716
L. Pan et al. (2019)	15.095	210.981	269.872
Wen et al. (2019)	18.61	85.55	–
L. Chen et al. (2019)	65.2	755.43	–
Ours	<b>8.057</b>	<b>74.4301</b>	<b>88.088</b>

**Table 2:** Inference Times of Algorithms on Different Datasets

Our approach achieves significant speed gains: up to **3** times compared to L. Pan et al. (2019), as presented in Table 2.

## 4.2.2 Visual Results

In this section, we present a visual comparison with other statistical deblurring algorithms using images from different domains, such as natural images, text images, low-light images, and images containing human face.



Fig. 5: Left to right: input image, followed by results from S. Cho and Lee (2009); J. Pan et al. (2016); Xu and Jia (2010) and our algorithm



Fig. 6: Left to right: input image, followed by results from S. Cho and Lee (2009); J. Pan et al. (2014b); Zhong et al. (2013) and our algorithm

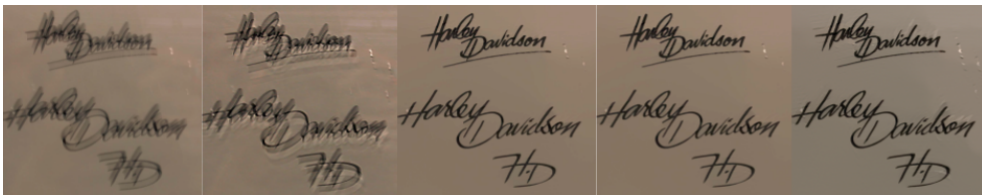


Fig. 7: Left to right: input image, followed by results from J. Pan et al. (2014b, 2016); Xu and Jia (2010) and our algorithm

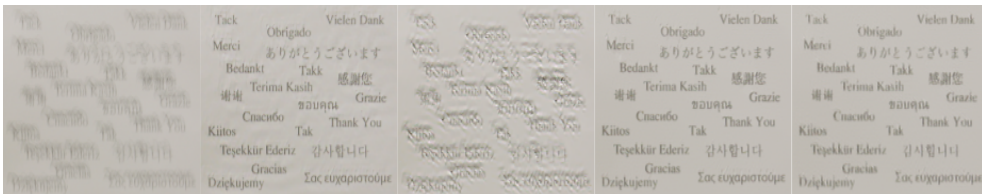
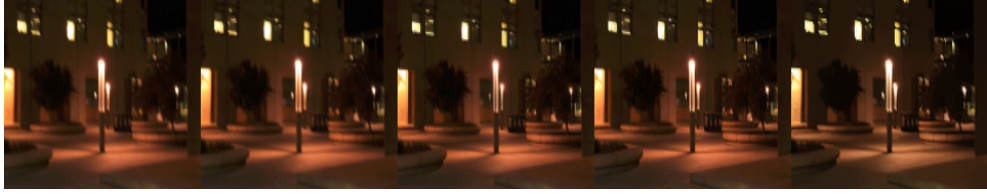


Fig. 8: Left to right: input image, followed by results from H. Cho et al. (2012); S. Cho and Lee (2009); J. Pan et al. (2014b) and our algorithm



**Fig. 9:** Left to right: input image, followed by results from [Hu et al. \(2014\)](#); [J. Pan et al. \(2016\)](#); [Xu and Jia \(2010\)](#) and our algorithm



**Fig. 10:** Left to right: input image, followed by results from [J. Pan et al. \(2014b\)](#); [Whyte et al. \(2012\)](#); [Xu and Jia \(2010\)](#) and our algorithm

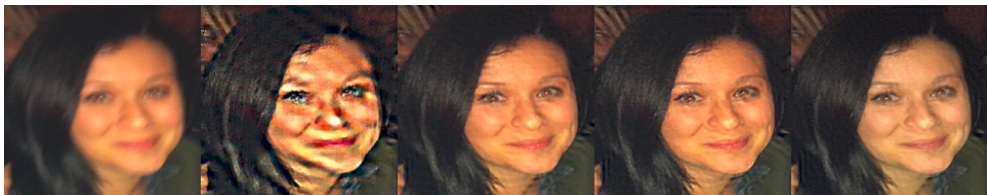


**Fig. 11:** Left to right: input image, followed by results from [J. Pan et al. \(2014a, 2016\)](#); [Xu and Jia \(2010\)](#) and our algorithm

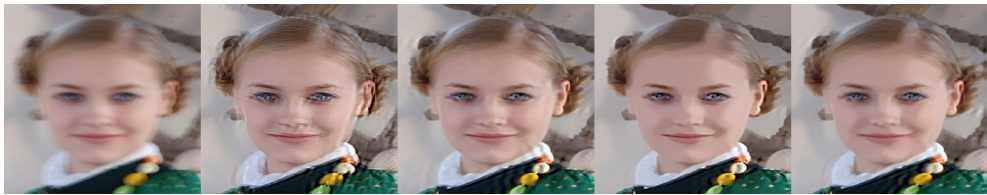


**Fig. 12:** Left to right: input image, followed by results from [J. Pan et al. \(2014b, 2016\)](#); [Xu and Jia \(2010\)](#) and our algorithm

Regardless of the domain that the image comes from, we obtain consistent results with improved image clarity (as seen in Figures 5, 6, 7, 8, 9, 10, 11, 12), which is a proof of the higher generalisation capabilities of our algorithm compared to other domain-specific methods.

### 4.3 Benchmarking with Transformer Based Deep Learning Algorithms

We conducted experiments using our algorithm as a post-processing unit in conjunction with the architecture, proposed in [Zamir et al. \(2022\)](#).

### 4.3.1 Quantitative Results

Using images from datasets provided by [Rim et al. \(2020\)](#); [Shen et al. \(2019\)](#) and [Nah et al. \(2017\)](#), we compare the PSNR and SSIM metrics of our deblurred results with those of other state-of-the-art algorithms based on transformer architectures to determine if our prior enhances the efficacy of this class of algorithms.

Model Name	RealBlur-J		RealBlur-R		HIDE		GoPro		Average	
	PSNR	SSIM	PSNR	SSIM	PSNR	SSIM	PSNR	SSIM	PSNR	SSIM
<a href="#">Zamir et al. (2022)</a>	28.96	0.879	36.19	<b>0.957</b>	<b>31.22</b>	<b>0.942</b>	32.92	0.961	32.3225	0.93475
<a href="#">Zamir et al. (2021)</a>	28.7	0.873	35.99	0.952	30.96	0.939	32.66	0.959	32.0775	0.93075
<a href="#">Tsai et al. (2022)</a>	28.82	0.876	36.08	0.954	31.03	0.939	<b>33.08</b>	<b>0.962</b>	32.2525	0.93275
<a href="#">L. Chen et al. (2022)</a>	<b>29.34</b>	<b>0.882</b>	35.01	0.928	19.38	0.62	26.76	0.898	27.6225	0.832
<a href="#">Kupyn et al. (2018)</a>	27.97	0.834	33.79	0.903	24.51	0.871	28.7	0.858	28.7425	0.8665
<a href="#">Kupyn et al. (2019)</a>	28.7	0.866	35.26	0.944	26.61	0.875	29.55	0.934	30.03	0.90475
<a href="#">K. Zhang et al. (2020)</a>	24.93	0.745	33.78	0.909	28.94	0.915	31.1	0.942	29.6875	0.87775
<a href="#">H. Zhang et al. (2019)</a>	28.42	0.86	35.70	0.948	29.09	0.924	31.2	0.94	29.57	0.918
Ours	28.99	0.88	<b>36.192</b>	<b>0.957</b>	<b>31.22</b>	<b>0.942</b>	32.92	0.961	<b>32.3305</b>	<b>0.935</b>

**Table 3:** PSNR and SSIM scores for different models across various datasets

As evidenced by the data in Table 3, our algorithm, when employed as a post-processing unit, consistently delivers superior performance on average across all datasets and achieves the best results on two of these datasets individually

### 4.3.2 Qualitative Results

Beyond quantitative analysis, a critically important factor in assessing image quality is its visual appeal and ability to convince an audience of its superiority. To address this, we designed a study where we presented sets of images to a group of participants for comparison and scoring.

- Type of Study:** The study is an online survey. A base image was used to generate deblurred images using our model and models from [L. Chen et al. \(2022\)](#); [Tsai et al. \(2022\)](#); [Zamir et al. \(2021\)](#); [H. Zhang et al. \(2019\)](#) and [Zamir et al. \(2022\)](#). The deblurred images were concatenated in a random order in a 3x2 grid without labeling. We show grids containing 10 sets of images to our participants and ask them to score them out of 10. A higher score implies a better image.
- Participants:** The participants were chosen at random from a set of volunteer participants. The set of random participants belongs to no specific educational background.
- Population Size:** A total of 76 people participated in the survey.
- Sampling Method:** The performance of our model was tested against a number of datasets, from [Nah et al. \(2017\)](#); [Rim et al. \(2020\)](#); [Shen et al. \(2019\)](#). The sample set of 10 base images was picked at random with an equal distribution among all the datasets.

Taking the scores out of 10, here are the average ranks for the models included in the survey.

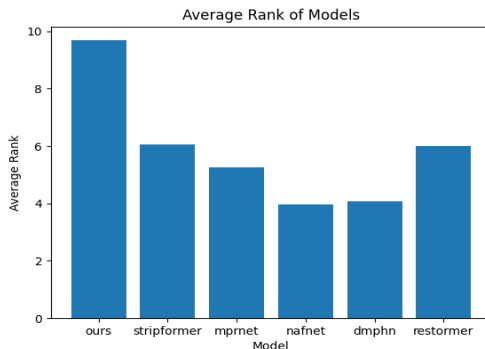


**Fig. 13:** Comparison of our model with state-of-the-art models

Here, we see in Fig. 13 that the results from our model obtained the highest score (over 9 out of 10, on average) among all the models in the discussion.

## 5 Conclusions and Future Work

In this paper, we propose a new prior for blind image deblurring, inspired by observations on the effects of convolution on image sparsity. We utilize Fourier transforms to extract frequency components, facilitating the separation of negative phases. This approach enabled the implicit determination of the blur kernel, informed by data on blur level and direction. The ReLU Sparsity prior is employed to penalize a higher  $L_0$  norm, which serves as an indicator of the blurriness of an image. To address the challenges associated with the non-convex optimization problem, we utilize half-quadratic splitting strategies. Our algorithm provides competitive performance on qualitative metrics such as PSNR, SSIM, and error ratio while providing upto three times lower inference times than the established state-of-the-art blind deblurring algorithms. Additionally, Our algorithm, serving as a post-processing unit, consistently outperforms competing methods, demonstrating its robustness and adaptability across a range of imaging conditions.

For future work, we plan to explore the integration of our algorithm’s rapid inference and portable framework with deep learning architectures to further enhance deblurring evaluations. Additionally, we aim to develop alternative mathematical strategies to reduce the computational demands associated with gradient descent in RFT image computation. Another area of focus will be leveraging inherent image attributes such as saturation, intensity, and illumination to optimize the estimation of multiple kernels, thereby improving the recovery of the latent image without compromising processing speed.



## Declaration

- **Funding:** The authors did not receive support from any organization for the submitted work.
- **Competing interests:** The authors have no competing interests to declare that are relevant to the content of this article.

## References

- Bai, Y., Cheung, G., Liu, X., Gao, W. (2018). Graph-based blind image deblurring from a single photograph. *IEEE Transactions on Image Processing*, 28, 1404-1418, Retrieved from <https://api.semanticscholar.org/CorpusID:3419385>
- Bai, Y., Jia, H., Jiang, M., Liu, X., Xie, X., Gao, W. (2019, 05). Single image blind deblurring using multi-scale latent structure prior. *IEEE Transactions on Circuits and Systems for Video Technology*, PP, 1-1, <https://doi.org/10.1109/TCSVT.2019.2919159>
- Chakrabarti, A., Zickler, T., Freeman, W. (2010, 07). Analyzing spatially-varying blur. (p. 2512 - 2519).
- Chan, T., & Wong, C.-K. (1998). Total variation blind deconvolution. *IEEE Transactions on Image Processing*, 7(3), 370-375, <https://doi.org/10.1109/83.661187>
- Chen, L., Chu, X., Zhang, X., Sun, J. (2022, 11). Simple baselines for image restoration. In (p. 17-33).
- Chen, L., Fang, F., Wang, T., Zhang, G. (2019). Blind image deblurring with local maximum gradient prior. *2019 IEEE/CVF Conference on Computer Vision and Pattern Recognition (CVPR)* (p. 1742-1750).
- Chen, X., He, X., Yang, J., Wu, Q. (2011). An effective document image deblurring algorithm. *Cvpr 2011* (p. 369-376).
- Chen, X., Yang, R., Guo, C., Ge, S., Wu, Z., Liu, X. (2020). Hyper-laplacian regularized non-local low-rank prior for blind image deblurring. *IEEE Access*, 8, 136917-136929, <https://doi.org/10.1109/ACCESS.2020.3010540>
- Cho, H., Wang, J., Lee, S. (2012). Text image deblurring using text-specific properties. *European conference on computer vision*. Retrieved from <https://api.semanticscholar.org/CorpusID:10376983>
- Cho, S., & Lee, S. (2009, 12). Fast motion deblurring. *ACM Trans. Graph.*, 28, , <https://doi.org/10.1145/1618452.1618491>
- Fergus, R., Singh, B., Hertzmann, A., Roweis, S., Freeman, W. (2006, 07). Removing camera shake from a single photograph. *ACM Trans. Graph.*, 25, 787-794, <https://doi.org/10.1145/1179352.1141956>

- Gupta, A., Joshi, N., Zitnick, C., Cohen, M., Curless, B. (2010, 09). Single image deblurring using motion density functions. (Vol. 6311, p. 171-184).
- Hirsch, M., Schuler, C., Harmeling, S., Schölkopf, B. (2011, 11). Fast removal of non-uniform camera shake. (p. 463-470).
- Hu, Z., Cho, S., Wang, J., Yang, M.-H. (2014). Deblurring low-light images with light streaks. *2014 IEEE Conference on Computer Vision and Pattern Recognition* (p. 3382-3389).
- Kim, K., Lee, S., Cho, S. (2022). *Mssnet: Multi-scale-stage network for single image deblurring*.
- Köhler, R., Hirsch, M., Mohler, B.J., Scholkopf, B., Harmeling, S. (2012). Recording and playback of camera shake: Benchmarking blind deconvolution with a real-world database. *European conference on computer vision*. Retrieved from <https://api.semanticscholar.org/CorpusID:262341811>
- Krishnan, D., Tay, T., Fergus, R. (2011). Blind deconvolution using a normalized sparsity measure. *Cvpr 2011* (p. 233-240).
- Kupyn, O., Budzan, V., Mykhailych, M., Mishkin, D., Matas, J. (2018). Deblurgan: Blind motion deblurring using conditional adversarial networks. *2018 IEEE/CVF Conference on Computer Vision and Pattern Recognition* (p. 8183-8192).
- Kupyn, O., Martyniuk, T., Wu, J., Wang, Z. (2019). Deblurgan-v2: Deblurring (orders-of-magnitude) faster and better. *2019 IEEE/CVF International Conference on Computer Vision (ICCV)* (p. 8877-8886).
- Lee-Thorp, J., Ainslie, J., Eckstein, I., Ontanon, S. (2022). *Fnet: Mixing tokens with fourier transforms*.
- Levin, A., Weiss, Y., Durand, F., Freeman, W.T. (2009). Understanding and evaluating blind deconvolution algorithms. *2009 IEEE Conference on Computer Vision and Pattern Recognition* (p. 1964-1971).
- Levin, A., Weiss, Y., Durand, F., Freeman, W.T. (2011). Efficient marginal likelihood optimization in blind deconvolution. *Cvpr 2011* (p. 2657-2664).
- Li, L., Pan, J., Lai, W.-S., Gao, C., Sang, N., Yang, M.-H. (2018). Learning a discriminative prior for blind image deblurring. *2018 IEEE/CVF Conference on Computer Vision and Pattern Recognition* (p. 6616-6625).
- Li, Z., Gao, Z., Yi, H., Fu, Y., Chen, B. (2023, 10). Image deblurring with image blurring. *IEEE Transactions on Image Processing, PP*, 1-1, <https://doi.org/10.1109/TIP.2023.3321515>
- Liu, J., Tan, J., He, L., Ge, X., Hu, D. (2020). Blind image deblurring via local maximum difference prior. *IEEE Access*, 8, 219295-219307, <https://doi.org/10.1109/ACCESS.2020.3039281>
- Ljubenić, M., & Figueiredo, M.A.T. (2017). Blind image deblurring using class-adapted image priors. *2017 IEEE International Conference on Image Processing (ICIP)* (p. 490-494).
- Mao, C., Liu, R., Li, H. (2018). Adaptive optimization with nested prior navigation for blind image deblurring. *2018 IEEE Fourth International Conference on Multimedia Big Data (BigMM)* (p. 1-7).

- Michaeli, T., & Irani, M. (2014, 09). Blind deblurring using internal patch recurrence. (Vol. 8691, p. 783-798).
- Nah, S., Kim, T., Lee, K. (2017, jul). Deep multi-scale convolutional neural network for dynamic scene deblurring. *2017 IEEE Conference on Computer Vision and Pattern Recognition (CVPR)* (p. 257-265). Los Alamitos, CA, USA: IEEE Computer Society. Retrieved from <https://doi.ieeecomputersociety.org/10.1109/CVPR.2017.35>
- Pan, J., Hu, Z., Su, Z., Yang, M.-H. (2014a, 09). Deblurring face images with exemplars. (p. 47-62).
- Pan, J., Hu, Z., Su, Z., Yang, M.-H. (2014b). Deblurring text images via l0-regularized intensity and gradient prior. *2014 IEEE Conference on Computer Vision and Pattern Recognition* (p. 2901-2908).
- Pan, J., Sun, D., Pfister, H., Yang, M.-H. (2016). Blind image deblurring using dark channel prior. *2016 IEEE Conference on Computer Vision and Pattern Recognition (CVPR)* (p. 1628-1636).
- Pan, L., Hartley, R., Liu, M., Dai, Y. (2019). Phase-only image based kernel estimation for single image blind deblurring. *2019 IEEE/CVF Conference on Computer Vision and Pattern Recognition (CVPR)* (p. 6027-6036).
- Rao, Y., Zhao, W., Zhu, Z., Lu, J., Zhou, J. (2021). *Global filter networks for image classification*.
- Rim, J., Haeyun, L., Won, J., Cho, S. (2020, 08). Real-world blur dataset for learning and benchmarking deblurring algorithms..
- Shan, Q., Jia, J., Agarwala, A. (2008, 08). High-quality motion deblurring from a single image. *ACM Trans. Graph.*, *27*, , <https://doi.org/10.1145/1360612.1360672>
- Shen, Z., Wang, W., Lu, X., Shen, J., Ling, H., Xu, T., Shao, L. (2019, 11). Human-aware motion deblurring..
- Sun, J., Cao, W., Xu, Z., Ponce, J. (2015, 06). Learning a convolutional neural network for non-uniform motion blur removal. (p. 769-777).
- Sun, L., Cho, S., Wang, J., Hays, J. (2013). Edge-based blur kernel estimation using patch priors. *IEEE International Conference on Computational Photography (ICCP)* (p. 1-8).
- Tao, X., Gao, H., Shen, X., Wang, J., Jia, J. (2018, June). Scale-recurrent network for deep image deblurring. *Proceedings of the IEEE Conference on Computer Vision and Pattern Recognition (CVPR)*.
- Tsai, F.-J., Peng, Y.-T., Lin, Y.-Y., Tsai, C.-C., Lin, C.-W. (2022, 11). Stripformer: Strip transformer for fast image deblurring. In (p. 146-162).
- Wang, Z., Cun, X., Bao, J., Zhou, W., Liu, J., Li, H. (2022, June). Uformer: A general u-shaped transformer for image restoration. *Proceedings of the IEEE/CVF Conference on Computer Vision and Pattern Recognition (CVPR)* (p. 17683-17693).
- Wen, F., Ying, R., Liu, P., Truong, T.-K. (2019, 06). *Blind image deblurring using patch-wise minimal pixels regularization*.
- Whyte, O., Sivic, J., Zisserman, A., Ponce, J. (2012, 06). Non-uniform deblurring for shaken images. *International Journal of Computer Vision*, *98*, 168-186, <https://doi.org/10.1007/s11263-011-0502-7>

- Xu, L., & Jia, J. (2010). Two-phase kernel estimation for robust motion deblurring. *European conference on computer vision*. Retrieved from <https://api.semanticscholar.org/CorpusID:8000561>
- Xu, L., & Jia, J. (2012). Depth-aware motion deblurring. *2012 IEEE International Conference on Computational Photography (ICCP)* (p. 1-8).
- Xu, L., Lu, C., Xu, Y., Jia, J. (2011, 12). Image smoothing via l0 gradient minimization. (Vol. 30, p. 1).
- Xu, L., Tao, X., Jia, J. (2014). Inverse kernels for fast spatial deconvolution. *European conference on computer vision*. Retrieved from <https://api.semanticscholar.org/CorpusID:5633112>
- Xu, L., Zheng, S., Jia, J. (2013). Unnatural l0 sparse representation for natural image deblurring. *2013 IEEE Conference on Computer Vision and Pattern Recognition* (p. 1107-1114).
- Yan, Y., Ren, W., Guo, Y., Wang, R., Cao, X. (2017). Image deblurring via extreme channels prior. *2017 IEEE Conference on Computer Vision and Pattern Recognition (CVPR)* (p. 6978-6986).
- Zamir, S.W., Arora, A., Hayat, M., Khan, F., Yang, M.-H. (2022, 06). Restormer: Efficient transformer for high-resolution image restoration. (p. 5718-5729).
- Zamir, S.W., Arora, A., Khan, S., Hayat, M., Khan, F.S., Yang, M.-H., Shao, L. (2021). Multi-stage progressive image restoration. *2021 IEEE/CVF Conference on Computer Vision and Pattern Recognition (CVPR)* (p. 14816-14826).
- Zhang, H., Dai, Y., Li, H., Koniusz, P. (2019, jun). Deep stacked hierarchical multi-patch network for image deblurring. *2019 IEEE/CVF Conference on Computer Vision and Pattern Recognition (CVPR)* (p. 5971-5979). Los Alamitos, CA, USA: IEEE Computer Society. Retrieved from <https://doi.ieeecomputersociety.org/10.1109/CVPR.2019.00613>
- Zhang, H., Wu, Y., Zhang, L., Zhang, Z., Li, Y. (2020, 02). Image deblurring using tri-segment intensity prior. *Neurocomputing*, 398, , <https://doi.org/10.1016/j.neucom.2020.02.082>
- Zhang, K., Luo, W., Zhong, Y., Ma, L., Stenger, B., Liu, W., Li, H. (2020). Deblurring by realistic blurring. *2020 IEEE/CVF Conference on Computer Vision and Pattern Recognition (CVPR)* (p. 2734-2743).
- Zhang, Z., Zheng, L., Piao, Y., Tao, S., Xu, W., Gao, T., Wu, X. (2022, 03). Blind remote sensing image deblurring using local binary pattern prior. *Remote Sensing*, 14, 1276, <https://doi.org/10.3390/rs14051276>
- Zheng, S., Xu, L., Jia, J. (2013, 12). Forward motion deblurring. (p. 1465-1472).
- Zhong, L., Cho, S., Metaxas, D., Paris, S., Wang, J. (2013). Handling noise in single image deblurring using directional filters. *2013 IEEE Conference on Computer Vision and Pattern Recognition* (p. 612-619).